The impact of sequential H_2-CO-H_2 activation treatment on the structure and performance of cobalt based catalysts for the Fischer-Tropsch synthesis.

Eleni Patanou[a*], Nikolaos E. Tsakoumis[a*], Rune Myrstad[b], Edd A. Blekkan[a]

[a] *Norwegian University of Science and Technology , Department of Chemical Engineering, NO-7491,Trondheim, Norway*

[b] *SINTEF Materials and Chemistry, Department of Oil and Gas Process Technology, Trondheim, Norway*

Corresponding Author

* E-mail : Eleni.Patanou@ntnu.no (E.P.), Nikolaos.Tsakoumis@ntnu.no (N.E.T.)

ABSTRACT

Different activation protocols were applied to a promoted Re/Co/γ-Al_2O_3 catalyst for Fischer-Tropsch synthesis. The activation included treatment in either pure H_2 or a sequence of Reduction (H_2) - Carburization (CO) - Reduction (H_2) in order to vary the microstructure of Co nanoparticles and investigate their performance. The alternative activation protocol applied under specific conditions (carburization at 230 ^oC and final reduction at 350 ^oC) outperform the conventional activation both in terms of catalyst activity and C_{5+} selectivity. The catalyst was characterized in all the stages of the activation process by synchrotron based X-ray diffraction (XRD) and X-ray absorption near edge structure spectroscopy (XANES). The effect of air exposure at room temperature of the carburized sample was investigated and it was found that air exposure leads to minor phase changes that significantly affect catalyst performance. Carburization temperature and temperature used for the decomposition of the carbide on the final reduction step both had a severe effect on catalyst performance, but neither of them influenced considerably the microstructure of Co nanoparticles that was primarily hexagonal (hcp). All carburized samples contained a significant amount of carbon as observed by Thermogravimetric analysis (TGA) and Raman spectroscopy. The final reduction step could remove part of the excess carbon produced during CO disproportionation. It appears that the carbon removal\minimization is a key factor for the exploitation of the benefits of hcp configuration of Co nanoparticles catalysing Fischer-Tropsch synthesis.

KEYWORDS Cobalt; Fischer–Tropsch; CO pre-treatment; Carburization; Cobalt carbide; Carbon effect

1. Introduction

Fischer – Tropsch synthesis (FTS) is the heart of the gas-to-liquids (GTL) process which is widely used for the utilization of synthesis gas deriving from natural gas, coal and biomass [1]. Particularly nowadays the increased development of unconventional gas sources such as shale gas, tight gas, and coal-bed methane[2] has led to a decline of the natural gas price, both in absolute terms and relative to crude oil, shifting further the focus towards this potential chemical route of producing fuels and chemicals from natural gas. Cobalt based catalysts appear as the most attractive choice for natural gas based FTS, because of their high activity, good stability and low water–gas shift activity [3,4]. FT catalyst activity and selectivity depends on several factors such as Co nanoparticle size, nature of the support, the presence of promoters, preparation methods and pre-treatment conditions [5].

The active phase in FTS when cobalt catalysts are used is metallic cobalt (Co^o) [6]. Typically, conventional catalyst precursors contain an oxide phase (Co_3O_4 spinel) dispersed on a refractory metal oxide that has to undergo activation in a reducing atmosphere at temperatures exceeding 300 ^oC [7]. Different activation routes include the direct exposure of the oxide or the reduced catalyst to hydrogen, synthesis gas or carbon monoxide [8,9]. The formation of metallic cobalt can alternatively be obtained by the decomposition of cobalt carbide (Co_xC) precursors under H_2.

Cobalt carbide precursors are prepared by CO disproportionation on metallic Co nanoparticles at atmospheric or high pressures, that are significantly reducing carburization time [10–19]. Two types of Co carbides are known, Co_2C and Co_3C, both orthorhombic structures. The role of cobalt carbide in FTS has been under consideration earlier by Hofer and Peebles [20], in an attempt to understand the mechanism of the FT reaction [21], while also focusing on its decomposition kinetics [22]. Cobalt carbide is the subject of many recent studies investigating the impact of the activation step on the catalyst

performance [16,17,19,23], the role of bulk cobalt carbide as possible deactivation mechanism [13,18], or as a possible precursor in temperature limited applications like continuous stirred tank reactor (CSTR) for catalyst testing [15]. However, carbon produced during carburization by CO disproportionation is not among the discussed topics.

It has been shown that decomposition of cobalt carbide primarily leads to hexagonal close packed cobalt nanoparticles, due to their structure similarity [10,11,24]. Catalyst activation, through cobalt carbide formation and decomposition has previously been reported as beneficial for the FTS activity [11,21], compared to the conventional H_2 reduction. The produced metallic cobalt hcp nanoparticles appear to have different FTS performance, possibly due to an altered CO activation pathway [25], higher number of active sites [14], or higher number of defects [19]. The impact of different cobalt phases in the catalyst performance is however still under debate. With a majority of studies focusing on catalyst activity alone, the important parameter of selectivity to higher hydrocarbons is often neglected. Therefore, there is a need to clarify the impact of the activation protocol on the catalysts structure and ultimately on catalyst performance with regard to C_{5+} selectivity, in order to achieve better catalyst design and process optimization.

This study demonstrates the condition sensitivity of the 3 step catalyst activation, including the sequence of Reduction (H_2) - Carburization (CO) - Reduction (H_2) (RCR), which may lead to improved or poorer FTS performance, when compared to the conventional H_2 reduction. The use of cobalt carbide as catalyst precursor is evaluated and its sensitivity against air is investigated. Carbon formation is evaluated by TGA and Raman as a side effect of the carburization process, and its influence on FTS catalysis is investigated and discussed.

2. Experimental

2.1. Sample preparation. A γ-alumina (Puralox SCCa, S_{BET} = 170 m^2/g, pore volume of 0.73 cm^3/g and 12 nm average pore size) supported catalyst containing 20 wt. % Co and 0.5 wt. % Re was prepared by incipient wetness (IW) co-impregnation with an aqueous solution of $Co(NO_3)\cdot 6H_2O$ and $HReO_4$. The catalyst was dried in an oven at 100 ^oC for 4 h and calcined in flowing air at 300 ^oC for 16 h with a ramping rate of 120 ^oC/h. The samples were sieved to a particle diameter of 53−90 μm. The catalyst underwent different activation protocols as described later in the text.

2.2. Catalyst characterization. Hydrogen chemisorption was performed using a Micromeritics 2020 unit at 40 ^oC. Prior to the analysis, the samples were reduced under H_2 flow at 350 ^oC for 10 h. The cobalt dispersion was calculated by assuming dissociative adsorption of H_2 on the cobalt metal surface [26] and that rhenium does not contribute to the amount of hydrogen adsorbed. Re acts as a promoter increasing the exposed surface area of Co [27]. The average cobalt metal particle size (d(Co^o) nm) was calculated from the Co metal dispersion (D%) by assuming spherical, uniform Co metal nanoparticles with a site density of 14.6 atoms/nm^2 [26].

Synchrotron X-ray based characterization was performed at the Swiss-Norwegian Beamlines (SNBL) located at the European Synchrotron Radiation Facility (ESRF) in Grenoble, France. Station BM01B was used for the combined XANES and XRD. For the measurements, a quartz capillary based *in situ* cell was used. The experiments were optimized for XRD and capillaries of 0.7 mm in diameter were used. A detailed description of the set up can be found in the literature [28].

X-ray absorption spectra were recorded at the Co K-edge (E = 7709 eV) using a double crystal Si (111) monochromator. The data collection was carried out in the transmission mode. Ion chamber detectors with their gases at ambient temperature and pressure were used for measuring the intensities of the incident (I_0) and transmitted (I_t) X-rays. Spectra from a cobalt foil (*hcp*) was used as $Co^{(0)}$ reference, while powder samples of pure Co_3O_4, CoO and $CoAl_2O_4$ were used as additional references. The energy calibration was done by measuring the spectrum of the cobalt foil with the energy of the peak of the first derivative as the edge energy (7709 eV). The Demeter software (0.9.24) from the Ifeffit software package (Version 1.2.11) [29], was used for the XAS data analysis. The simulated XANES spectra have been constructed by *ab initio* simulations using the FDMNES package [30], when applicable the output from XRD refinement was used as input for the construction of the models.

X-ray diffractograms were obtained in an alternating sequence with XAS measurements using two independent Si (111) monochromators. XRD data were collected with the standard BM01B set-up, using a wavelength λ of 0.505 Å. A Si (111) standard was used for beam calibration. 2D images were obtained from a Dexela 2923 two-dimensional CMOS X-ray detector and converted to normal diffraction patterns using the program FIT2D [31]. An estimation of the mean cobalt crystallite size was obtained using the Scherrer formula [32] Average FWHM was obtained from pattern decomposition by the Pawley and Le Bail methods [33], applied with Fityk 0.9.8 program [34] and TOPAS v4.2 [35] software.

Thermo-gravimetric analysis (TGA) of the carburized samples coupled with differential scanning calorimetry (DSC) and mass spectrometry (MS) were used to study the mass loss, due to the removal of carbon of the carburized samples during reduction in H_2 and subsequent oxidation in air. TGA–MS analysis was carried out using a Jupiter STA 449C from Netzsch. In addition, the heat flow was monitored by the integrated DSC. The gases that evolved during the heating process were mon-

itored with the quadrupole mass spectrometer. The samples (~20 mg) were treated initially in flowing H_2 (10 mL/min) and Ar (30 mL/min) from 30 to 350 ^oC for 10 h, at a rate of 5 ^oC/min. The system was allowed to cool under Ar flow. Subsequently the samples were heated under air flow (100 ml/min) with a heating rate of 3 ^oC/min from 30 to 900 ^oC, for 5 hours. Argon was used as protective gas (25 mL/min) in both steps.

Raman spectra have been acquired by a Horiba Jobin Yvon LabRAM HR800 spectrometer. A He–Cd laser (325 nm) was used as excitation source. The laser power was reduced to 0.3 mW by applied filters and the beam was focused on the sample with a 40× objective. Spectra obtained with 20 second exposure and multiple acquisitions were averaged.

2.3 Catalyst activation. The activation procedure consisted of a sequence of 3 steps (RCR). A primary reduction step in H_2 (R), secondly a carburization step (C) of the metallic nanoparticles and finally a secondary H_2 reduction (R), prior to the catalyst exposure at FTS conditions. The reference sample underwent only the first reduction step in H_2, and the subsequent FTS experiment was undertaken according to a standard procedure [36]. Some of the samples were exposed to air for 30 minutes after the carburization step, either in static atmosphere at room temperature or under a flow of synthetic air. The catalyst was then reduced in flowing H_2 before the FTS experiment. The activation of the samples was performed in a 10 mm i.d. steel tube fixed-bed reactor. The catalyst bed was diluted with twenty parts per weight of SiC (75–150mm) for one-part catalyst to reduce the temperature gradients throughout the catalyst bed. For the air exposed samples the dilution took place after a sample of the carburized catalyst mass was taken to be characterized. Subsequently, the remaining sample was reloaded to the fixed-bed reactor for the following steps. Aluminium blocks were fixed around the steel tube reactors to improve the heat distribution in the axial direction, and the reactors were placed in a furnace. 3 thermocouples along the catalyst bed were used for temperature monitoring and control. In the first reduction step (identical for all the samples), the samples were treated with pure H_2 at 350 ^oC for 10 h with a ramping rate of 60 ^oC/h. In the carburization step the reduced catalyst was exposed to pure CO (250 mL·min−1·gcat−1), at either 230 ^oC or 300 ^oC. The reactor was first pressurized with Ar to 14 bar. Then CO was introduced by replacing the Ar flow gradually, in order to keep the temperature increase in the catalyst bed below 2 ^oC during the carburization.

2.4 Fischer – Tropsch Synthesis. FTS was carried out in tubular fixed-bed reactors, at 210 ^oC and 20 bar pressure with a H_2/CO ratio of 2.1. The followed procedure was identical so as to be able to compare the results with the reference catalyst. Initially the sample (carburized or oxide) was treated with H_2 at 1 bar for 10 h with a ramping rate of 60 ^oC/h. The reduction temperature was either 200 ^oC or 350 ^oC. After the reduction the catalyst was cooled to 170 ^oC and pressurized with He to 20 bar before the syngas feed of 250 Nml/min was introduced. Heating to the target temperature was done gradually. The sample was heated first to 190 ^oC with a ramping rate of 30 ^oC/h, then to 200 ^oC with a ramping rate of 5 ^oC/h, and finally to the target temperature of 210 ^oC with a ramp rate of ∼6 ^oC/h. To collect wax and liquid products, one hot trap at ∼85 ^oC and a cold trap at ambient temperature were used. Gas-phase products (after the traps) were fed into an HP 6890 gas chromatograph with a GS−Alumina PLOT column, a thermal conductivity detector (TCD), and a flame ionization detector (FID). The synthesis gas contained 3% N_2, which served as an internal standard for quantification of the products. After 24 h time on stream (TOS) at a fixed space velocity the catalyst activity was determined before the space velocity of the feed gas was adjusted (after about 30 h TOS) to obtain 50 ± 5% CO conversion in order to record selectivity data at a fixed conversion level. The selectivity data reported here are collected at similar conversion levels (46-47%) based on the analysis of C_1−C_4 hydrocarbons in the gas phase. Since the desired products are higher hydrocarbons, the selectivity is reported as C_{5+} and CH_4 selectivity. In the cases where carburized catalysts were extracted from the reactor and weighed before being reloaded in the reactor the mass used in the calculation was corrected with respect to the weight difference of cobalt carbide (Co_2C) and cobalt oxide (Co_3O_4) and the total deposited carbon that has been calculated from the thermogravimetric analysis.

3. Results and discussion

A calcined Re/Co/γ-Al_2O_3 catalyst prepared by IW impregnation was used as a precursor for the investigation of the effect of an alternative RCR activation procedure. Re promoter was used in order to achieve high degree of reduction, eliminating the contribution from remaining Co oxidic phases. The sample was subjected either to conventional activation under H_2 (sample denoted here as reference) or to the 3 step activation sequence (RCR), before it was tested under FTS conditions (15000 Nml/h•g, 210 ^oC, 20 bar, H_2/CO=2.1). The FTS activity was compared after 24 h on stream, while the selectivity was compared at similar conversion levels (46-47%) in order to eliminate effects of pH_2O [37]. All the samples were reduced at 350 ^oC prior to the carburization step. Different carburization protocols were used, performing the carburization at 230 ^oC or 300 ^oC and the final reduction step at 200 ^oC or 350 ^oC. Air exposure of the carburized sample was evaluated for exploiting potential use of a carburized catalyst as precursor (storage, transfer and *in situ* activation), for example in a continuous stirred-tank reactor (CSTR), where catalyst activation in the gas-phase can be a challenge. Characterization of the cobalt oxide precursor (Co_3O_4) and cobalt carbide produced by CO carburization was performed by H_2 chemisorption, XRD and

XANES. Carbon deposition on the carburized samples was evaluated by a TGA-DSC-MS and Raman spectroscopy. A summary of the samples tested and the 3 step activation conditions are presented in **Table 1**.

Table 1. Catalyst samples and activation conditions.

	Primary reduction T(°c)	Carburization* T(°c)	Air Exposure	Final reduction T(°c)
REFERENCE	350	-	-	-
230C-350R	350	230	-	350
230C-AIR-350R (1)	350	230	Static/atm air	350
230C-AIR-350R (2)	350	230	Static/atm air	350
230C-AIR-350R (3)	350	230	Flow/synthetic air	350
230C-200R	350	230	-	200
230C-AIR-200R	350	230	Static/atm air	200
300C-350R	350	300	-	350
300C-AIR-350R	350	300	Static/atm air	350

* P = 14 bar for 3h, under pure CO (99.97%)

3.1. Cobalt oxide precursor (Co_3O_4). Characterization of the calcined catalyst shown in Figure 1 confirms that the Co nanoparticles (NPs) primarily adapt a Co_3O_4 spinel structure after calcination at 300 °C. The Pawley method was applied and the full width at half maximum (FWHM) was determined for all diffraction peaks by using Lorenzian functions, allowing the calculation of the mean crystallite size by the Schrerrer equation. Co_3O_4 NPs of an average size of 16.5 nm where found, indicating that metallic Co NPs will be approximately 13.2 nm due to shrinkage from O removal from the lattice [38], assuming that no particle break-up is taking place during reduction.

The sizes are in agreement with Co particle size obtained from dispersion (11.7 nm) and near the pore size of the γ-Al_2O_3 support. The particle size is above the size sensitivity regime [39,40], that may influence interpretation of the results. The diffraction pattern was decomposed by using the cubic F*d*-3m crystal phases of Co_3O_4 NPs and γ-Al_2O_3 support. The refined lattice constants are equal to a = 8.0654 Å for the Co_3O_4 and a = 7.8920 Å for the support (R_{wp} = 4.77).

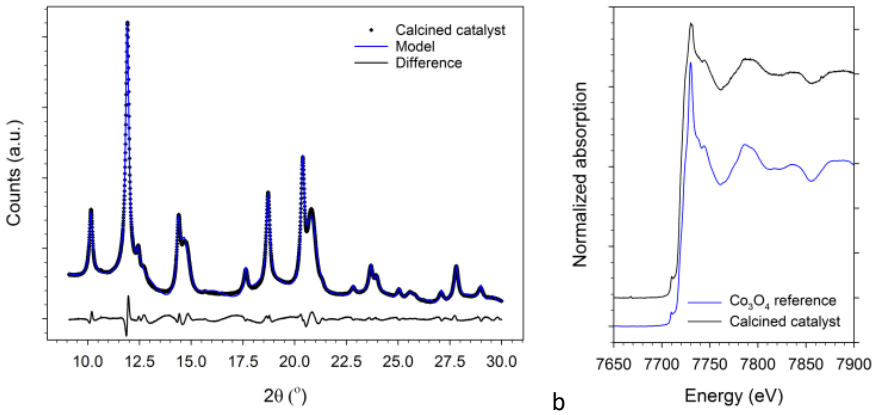

Figure 1. *a) X-ray diffraction pattern (λ = 0.505 Å) and simulated pattern consisting Co_3O_4 and γ-Al_2O_3 phases, (b) XANES of the calcined Re/Co/γ-Al_2O_3 catalyst and Co_3O_4 reference compound.*

3.2. Cobalt carbide precursor (Co_2C). X-ray analysis on the air exposed carburization products that had not undergone the last reduction step (noted here as 230C and 300C) can be seen in Figure 2. The diffraction patterns were normalized to the

(044) reflection of γ-Al_2O_3 using it as internal standard, assuming that γ-Al_2O_3 is fully retaining its structure during the carburization process, a fact that is supported by the obtained lattice parameter of γ-Al_2O_3 that is equal to 7.893 ± 0.0015 Å for calcined catalyst and the carburized samples. Nevertheless, differences in the diffraction patterns are evident for the samples carburized at different temperatures. In particular, although both catalysts contain predominantly γ-Al_2O_3 (F*d*-3m) and Co_2C (Pmnn) structures, the catalyst carburized at higher temperature has an additional minor contribution from the face-centred cubic (fcc) metallic cobalt phase. It is also noteworthy that contributions from Co_3C could not be detected. Pattern refining showed very similar crystallite sizes for the crystalline carbide particles near 8.5 nm for both samples. The refined lattice parameters for Co_2C that was formed at low and high carburization temperatures are presented in **Table 2**.

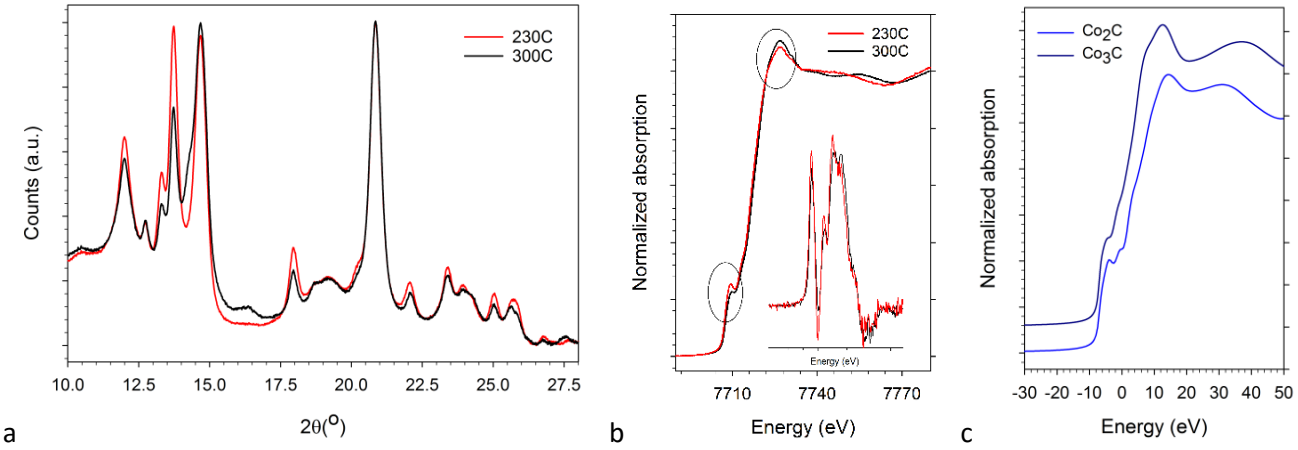

Figure 2. *(a) X-ray diffraction patterns of the air exposed carburized samples at 230 and 300 °C (λ=0.505 Å), (b) Co-XANES on the K-edge of the air exposed carburized samples at 230 and 300 °C and their derivatives; inset, (c) simulated Co-XANES spectra of Co_2C and Co_3C.*

Co-XANES at the K-edge of both low and high temperature carburization samples Figure 2b exhibit similarities. In both spectra an intense pre-edge shoulder is followed by a second smoother shoulder and a "white line", all characteristics can be found in *ab initio* calculated Co_3C and Co_2C carbide structures as illustrated in Figure 2c. Only in the later XANES region above 7740 eV noticeable differences can be seen. Apparently, the differentiation of the contribution of the Co phases in the XANES spectra is difficult since metallic Co and possible Co_xC have rather similar features. In addition, any contribution from remaining oxides further complicates the analysis.

Table 2. Refined unit cell parameters from the two produced carbides.

	Phase	Space group	A (å)	B (å)	C (å)	Rwp	Crystal size
230C	Co_2C	Pmnn	4.3630	4.4616	2.8724	5.91	8.5
300C	Co_2C	Pmnn	4.3650	4.5919	2.8394	2.42	8.5

3.3. Air stability of Co_2C. The sample carburized at 300 °C (and prior to the last reduction step, denoted as 300C) was exposed to air during transfer and inserted into the *in situ* cell for sequential XRD and XANES analysis *in situ*. It was further exposed to a mixture of 20% O_2 in He for 2 h at ambient temperature. The diffraction patterns that were obtained in the start and the end of the treatment are identical. Their subtraction reveals no changes in the crystal structure of the sample (Figure 3a). From the obtained XRD patterns it appears that the air exposed carbide is stable in air, in accordance to similar observations by Kwak et al. [15] In contrast, the Co-XANES shows a minor phase change occurring during the course of the O_2 treatment at room temperature (Figure 3b). The changes in the spectral features are initiated after 35 min in O_2 at 7725eV while changes at 7762 eV, 7742 eV and 7717 eV follow. It should be noted that the CoO phase has an intense "white line" peaking at 7724 eV. XANES analysis probes all Co containing species independent of their crystallinity. The exact nature of the formed phase is difficult to describe accurately from the present dataset, however the sensitivity of the Co_2C in air at room temperature is demonstrated. The modification of the carbide surface from O_2 exposure has an effect on the catalyst performance as will described later, this renders the previously proposed direct use of carburized sample or in its passivized state as catalyst precursor problematic.

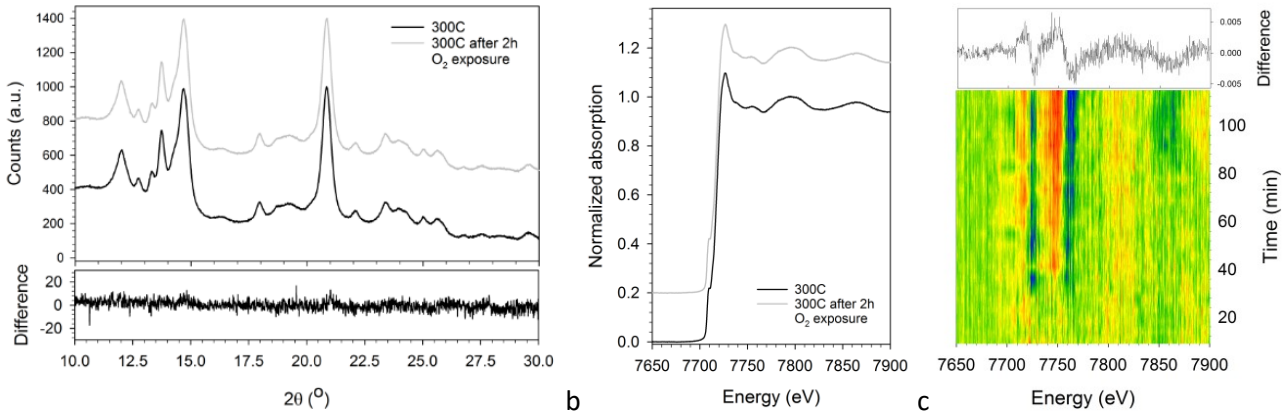

Figure 3. *Air stability of the carburized sample at 300 °C (300C) before and after exposure to a mixture of 20% O_2 in He for 2 h together with their difference (a) X-ray diffraction patterns (λ = 0.505 Å), (b) Co-XANES on the K-edge, (c) contour plot of differential XANES (ΔXANES) of the normalized spectra shows the slow development of the phase formed; first minus last scan (up).*

3.4. Fischer-Tropsch synthesis activity and selectivity performance. The FTS activity (reported as the CO reaction rate) varies over a wide range demonstrating a rather strong effect of the RCR activation process. At a carburization temperature of 230 °C it is apparent that the RCR protocol has the best overall performance (230C-350R), when the second reduction step is done at 350 °C. The CO reaction rate ($-r_{CO}$) is significantly higher (a 54% increase) on the catalyst that followed the RCR activation procedure without any air exposure (Figure 4, closed circle) as compared to the reference. The positive effect of the RCR pre-treatment on catalyst activity has been observed previously, even at higher magnitudes than the present result [11,13,15]. In addition, a remarkable enhancement of the C_{5+} selectivity is observed, a 5% increase and apparently linked to reduced methane selectivity (Figure 5a). There is also a large increase (32%) in the olefin paraffin ratio for the C_3 hydrocarbons (Figure 5b, closed circle).

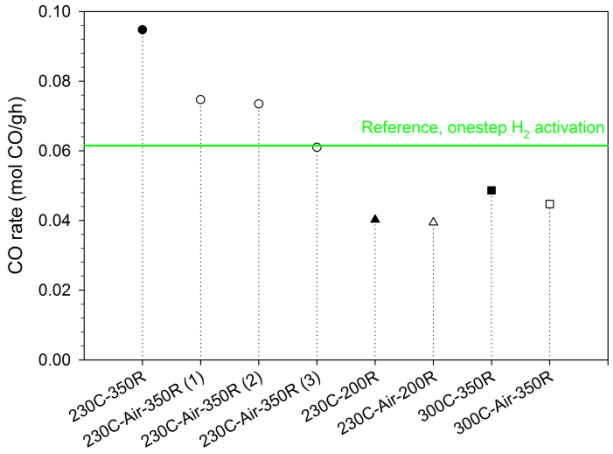

Figure 4. *Effect of the RCR activation protocol on CO reaction rate after 24h under FTS (210 °C, 20 bar, GHSV=15000 Nml/h•g, H_2/CO=2.1). The reference catalyst, which underwent conventional H_2 reduction activation, is denoted with green.*

Evaluation of air exposure was done for the sample carburized at 230 °C either by removing the catalyst and re-loading it into the reactor, after being exposed at ambient atmosphere at room temperature for approximately 30 min (samples 230C-Air-350R (1) and 230C-Air-350R (2), respectively) and by flowing synthetic air (20 % O_2 in N_2) for 30 min (sample 230C-Air-350R (3)). "Atmospheric" air exposure has a small but significant negative effect on the reaction rate as can be seen in Figure 4, open circles. However, the sample exposed to a flow of synthetic air (230C-Air-350R (3)) is more strongly affected, and has the same activity as the reference catalyst, significantly lower than when the air exposure occurs by exposure to the atmosphere (hence by diffusion alone). With respect to the C_{5+} selectivity air exposed catalysts cluster at slightly lower selectivities compared to the sample that was carburized and not exposed to air before reduction, (Figure 5, open circles), but still higher than that of the reference. Concerning the olefin/paraffin ratio of the C_3 hydrocarbons, the performance of the air exposed samples fall between the values of the non-exposed catalyst and the reference.

Decomposition of the carbide at 200 ^{o}C (230C-200R) leads to a poorer catalyst performance. Both the catalyst activity and the C_{5+} selectivity are lower than that of the reference (Figure 5, triangles). In fact, the reaction rate measured for the sample 230C-200R was the lowest in the current dataset (Figure 4, closed triangle). However, the olefin/paraffin ratio is high. This could be attributed to the effect of carbon deposits, as a correlation between carbon deposits and increased product olefinicity has been reported previously [41]. Air exposure of the carbide leads to a slightly higher reaction rate compared with the non-exposed sample, but also to an enhanced C_{5+} selectivity and C_3 o/p ratio (Figure 5, open triangle).

The samples that received the RCR pre-treatment at a carburization temperature of 300 ^{o}C (300C-350R) showed a poor catalytic performance (Figure 5, squares). Low reaction rates and poor C_{5+} selectivities were measured. The air exposure in this case had a positive effect on the C_{5+} selectivity and on the C_3 o/p ratio (Figure 5, open square), as well as on the CO reaction rate, which was positively affected (Figure 4, open square). The suppressed catalytic behaviour found for the samples with potentially higher carbon content, either due to lower H_2 reduction temperatures or due to high carburization temperatures, suggests a strong influence of carbon on the catalyst performance, but the effect on the C_3 o/p is more scattered and unclear.

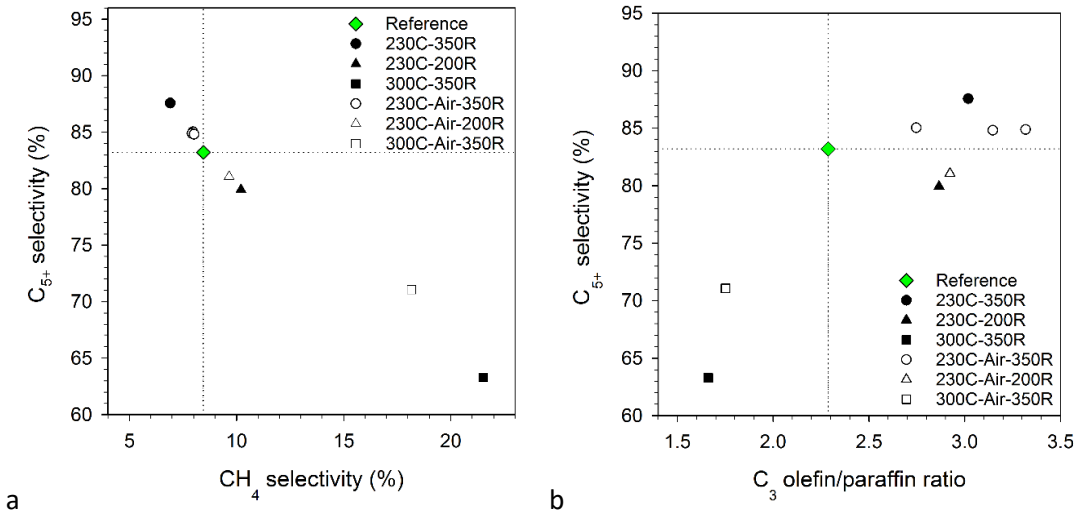

Figure 5. *Effect of the RCR activation protocol on selectivity under FTS (210 ^{o}C, 20 bar, H_2/CO=2.1) reported approximately after 70 h TOS at a CO conversion of 46-47% (a) C_{5+} selectivity with CH_4 and (b) C_{5+} selectivity with C_3 olefin/paraffin ratio.*

3.5. Catalysts Stability. After multistage activation and FTS the wax covered spent catalysts, (samples 230C-350R and 300C-350R) were collected, separated from the SiC diluent and analyzed by X-ray diffraction. The XRD analysis confirms that both these catalysts, that underwent the RCR activation procedure, have primarily cobalt in a hcp crystal configuration. The (010), (002), (011) and (012) reflections of hcp-Co can be seen in Figure 6. Sharp diffraction peaks from crystalline wax and remaining SiC can be seen together with broader contribution from the γ-Al_2O_3 support. It becomes evident that the hcp structure is preserved during the FTS run, while the deactivation rates are similar for the catalysts independently of the activation protocol applied.

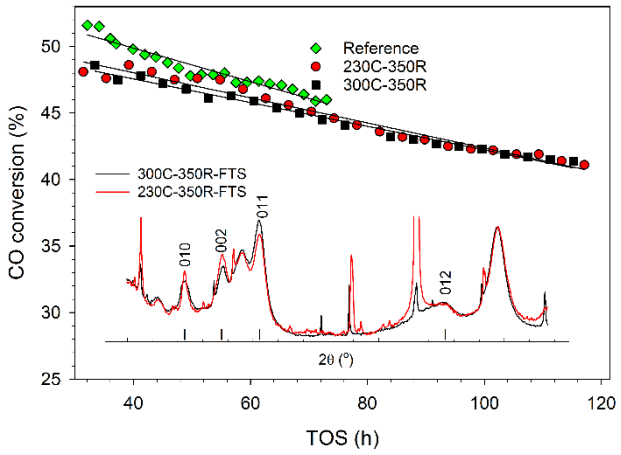

Figure 6. *Catalyst stability for both carburization temperatures (230 and 300 °C) compared to the reference. Deactivation profiles expressed as % CO conversion with TOS, (inset) X-ray diffraction patterns (λ = 0.505 Å) of the spent samples; indexes refer to hcp cobalt.*

3.6. Final reduction product. The last stage of the multistep activation is carbide decomposition under a H_2 atmosphere, which provides the actual active phase. Here, results for identical decomposition temperature to the first reduction step (350 °C) are presented. From the XRD of catalysts activated in H_2 and under the RCR process a clear difference in the crystal structure can be seen in Figure 7a,b. Cobalt is primarily found in an fcc configuration (with a minor presence of hcp) when a direct H_2 activation is applied. Stacking disorders and the co-existence of both cobalt phases renders a very challenging structure refinement. On the contrary a hcp configuration is adapted when the RCR activation process is used, as was observed very early by Weller et al. [20,21] and confirmed later for various cobalt based catalytic systems [12]. Diffraction analysis of the final catalyst showed a crystallite size of 7.3 nm of hcp Co for the sample carburized at 230 °C and 8.2 nm for the sample carburized at 300 °C. Any contribution from fcc cobalt is absent in the sample carburized at 230 °C, and barely visible on the catalyst carburized at 300 °C, at (002) 16.33° (2θ). The Co NP size obtained from the dispersion measurements through H_2 chemisorption of sample 230C was found significantly larger (11.9 nm) suggesting that part of Co might be amorphous (XRD invisible) or substantial structure disorder exists, resulting in peak broadening and subsequent size underestimation (**Table 3**).

Table 3. Crystallite and particle sizes at different parts of the activation for sample carburized at 230 °C as obtained by XRD and H_2 chemisorption, respectively.

	Dominant phase	**Crystallite size (XRD)**	**Particle size (H_2 chem.)**
CALCINATION	Co_3O_4	16.5 nm	
1ST REDUCTION	fcc-Co	13.2 nm*	11.7 nm
CARBURIZATION	Co_2C	8.5 nm	
2ND REDUCTION	hcp-Co	7.3 nm	11.9 nm

*Volume based calculation according to Rønning et al. [38]

XANES spectra of the carburized samples after the final H_2 reduction are almost identical, resembling the XANES spectrum of Co hcp foil suggesting highly extended reduction Figure 7c. The degree of reduction was evaluated by linear combination of reference samples (Co foil, CoO and $CoAl_2O_4$) and found 92% (±5) for both samples.

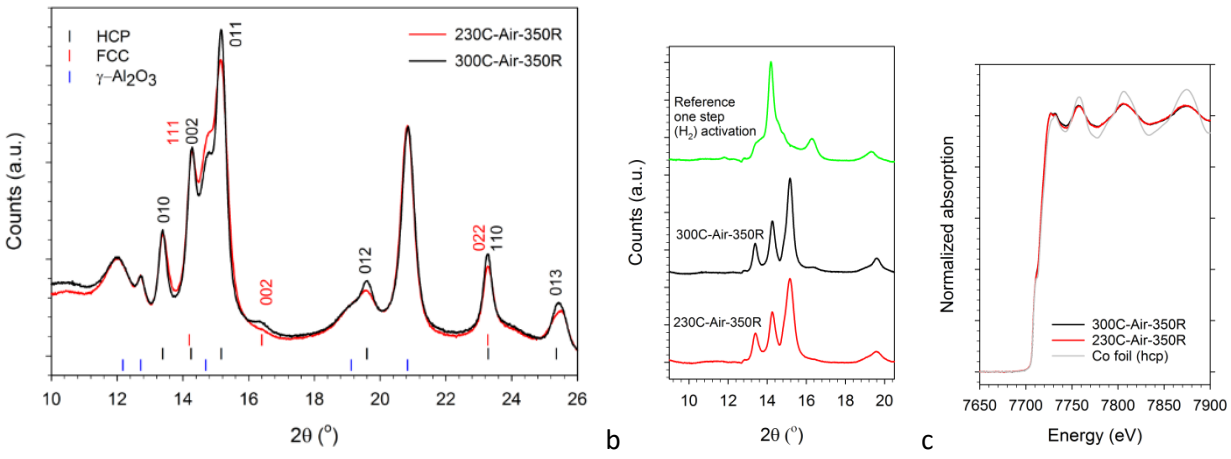

Figure 7. *Decomposition of the carbide at 350 °C for both carburization temperatures (230 and 300 °C) (a,b) X-ray diffraction patterns (λ = 0.505 Å), (b) XRD patterns with γ-Al_2O_3 support subtracted (c) Co-XANES at the K-edge.*

3.7. Evaluation of carbon deposition. Carbon formation from CO treatment has not been a major topic in published work primarily focusing on the crystallographic nature of cobalt NPs. Upon exposure to CO part of the gas will dissociate on the Co surface and, depending on the conditions, a fraction may directly be transformed to solid carbon through the exothermic Boudouard reaction $2CO_{(g)} \leftrightarrow CO_{2(g)} + C_{(s)}$ [42]. In some carburization experiments, we experienced temperature runaway phenomena that would support the importance of this reaction.

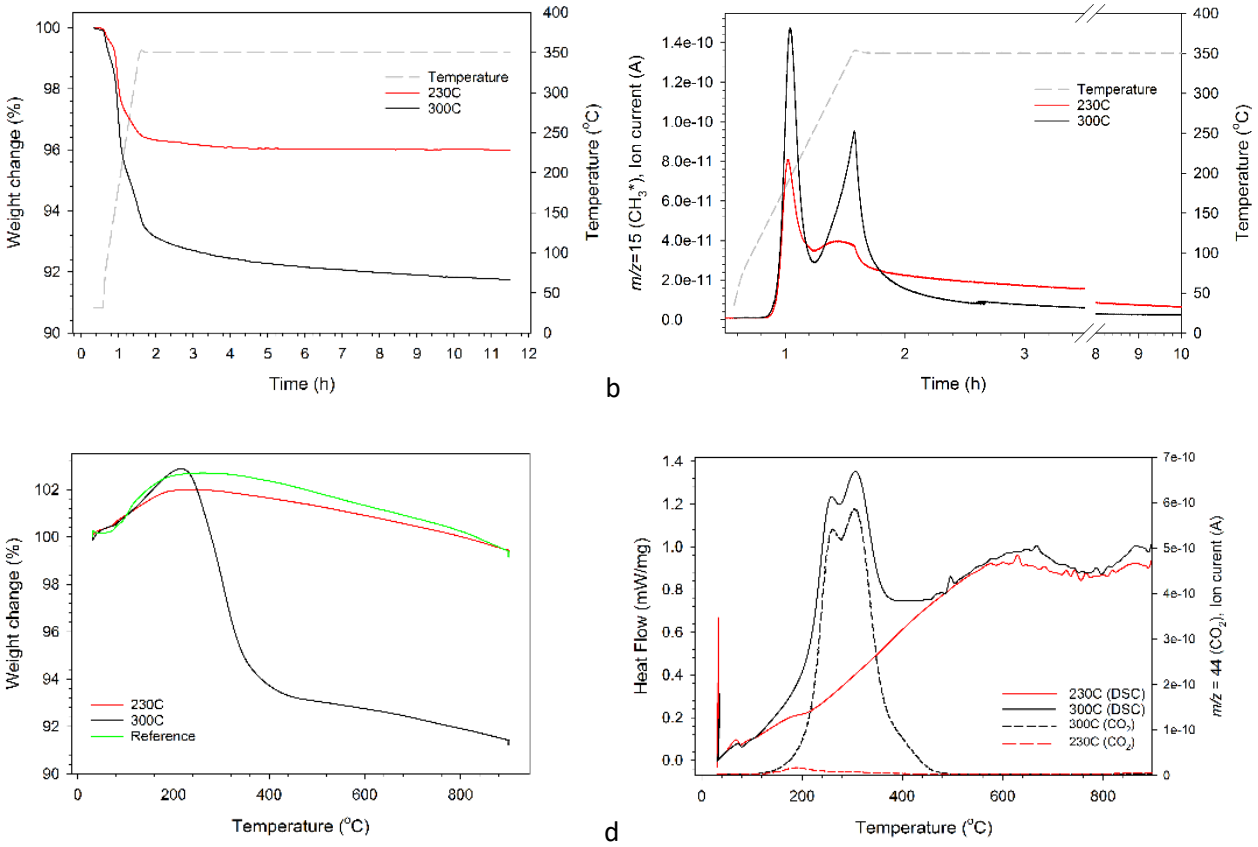

Figure 8. *TGA-DSC-MS signal obtained for the carbides 230C and 300C during the H_2 reduction step (a) TGA as f(t) in H_2 (b) CH_4 (m/z = 15) formation as f(t) in H_2; and during the subsequent oxidation step (c) TGA as f(T) in air, (d) DSC and CO_2 formation (m/z=44) both as f(T).*

Presumably, the subsequent steps leading to the carbide involve the diffusion of atomic C inside the Co NP which will create carbidic structures (subsurface or bulk) and/or the formation of carbon structures through C-C coupling in the outer surface of the Co NP. The adsorbed oxygen on the surface can be removed as CO_2. Qualitative and quantitative characterization of the nature of carbon deposits is critical for the following three reasons: a) the error that is introduced in catalyst weight and weight normalized reaction rates, b) the loss of active surface area and c) the understanding of the performance influence with respect to the type of carbon structure. It has previously been demonstrated that carbon has a negative (deactivating) effect on the FTS activity [42], and selectivity [40]. Also, a more unclear positive effect on olefin selectivity has been reported [41]. Here our efforts are towards quantitative evaluation of the carbon, contained in the carburized catalysts that are weighed and used as precursors (samples 230C and 300C) and to obtain a basic understanding of key features of the carbon formed.

To achieve this a combined TGA-DSC-MS measurement of the carburized samples was used. First the conventional H_2 reduction protocol was followed in order to show how much of the carbon can be hydrogenated at the applied reduction conditions. It appears that both carburized samples show significant amount of CH_4 formation during reduction in H_2. The weight loss curve (Figure 8a) shows a rapid weight loss during the heating period for both samples, with a change in the rate around 300 ^oC and a slow almost linear weight-loss during the temperature hold at 350 ^oC. The corresponding CH_4 signal shows similar pattern for both samples consisting of two features, a first peak at around 196 ^oC and a more complex shape initiated above 280 ^oC. The first part of the analysis is followed by a slow decline in the methane formation rate, approaching zero towards the end of the experiment. This suggests the presence of surface/atomic carbon (C_α), bulk carbidic (C_γ) and polymeric carbon (C_β) species, as classified by Bartholomew [43]. In particular for the 230C carbide sample the CH_4 production has its maximum at approximately 196 ^oC and 320 ^oC (Figure 8b), which suggests the existence of atomic and polymeric carbon, in addition to the expected carbidic phase that has been detected by XRD (Figure 2a). Similar peaks can be found in the sample carburized at 300 ^oC. This sample contains a higher amount of carbon that can be hydrogenated at high temperatures (exceeding 250 ^oC), seen as a larger peak area. The following carbon oxidation step (Figure 8c, d) clearly shows large amounts of CO_2 forming from the catalyst carburized at 300 ^oC.

Table 4. Mass loss of the carbides stored in air obtained from thermogravimetric analysis.

	H_2 reduction **Mass loss** (%)	**Air oxidation** **Mass loss** (%)
230C	4.00	< 0.5
300C	8.06	8.21

Evidently, a large amount of carbon (8.2 wt.%) unreactive to H_2 under the specific conditions applied exists during FTS on the catalyst carburized at high temperatures, while there is a minor amount of unreactive carbon on the 230C carbide (<0.5 wt.%); **Table 4**. For the 300C carbide encapsulation of the Co particles might explain its poor performance and the observed reduction in the Co surface area (dispersion of 2,6 % from H_2 chemisorption). In addition, the remaining amorphous or subsurface carbon might explain the lower rates detected in the 230C-200R FTS run. It has been shown that surface and subsurface carbon on cobalt may influence the adsorption characteristics of CO and consequently its dissociation affecting the reaction rates [42].

Raman scattering spectroscopy was used in order to provide input on the different structures of carbon in the carburized samples (230C and 300C). Raman excitation in the near UV region (325 nm) was applied for avoiding fluorescence background from the γ-Al_2O_3 and to enhance the sensitivity. The laser power was decreased by two orders of magnitude with neutral filters to diminish photo- or heat-induced transformations [44]. Indeed, the 20 second exposure of the material under the laser beam did not form detectable Co-O bonds, suggesting that laser induced oxidation of cobalt that could lead decomposition of the Co_2C structures and graphitic structures did not take place. Nevertheless, it should be noted that possible gradual oxidation of Co by air as has been detected by *in situ* XANES (see Figure 3) might have affected the structure of carbon. In addition, any photo-induced transformation of molecular carbon structures cannot be excluded [45].

The acquired spectra from the carburized samples appear significantly different from the reference (calcined) catalyst. As mentioned above there is an absence of Co-O vibrations at 680 cm^{-1}, suggesting that the carbides retain their structure. In the region above 1000 cm^{-1} the spectra differ significantly from the reference calcined catalyst providing further proof for the existence of carbon; Figure 9. Carbon structures have characteristic features in their Raman spectra from which infor-

mation on the sp^2 hybridization of carbon and consequently the carbon-carbon bonding can be extracted. The G band at around 1500 to 1700 cm^{-1} and the D band at around 1250 to 1450 cm^{-1} are the most prominent features, related to the vibrational modes (stretching and breathing) of sp^2 carbons in rings and chains [46].

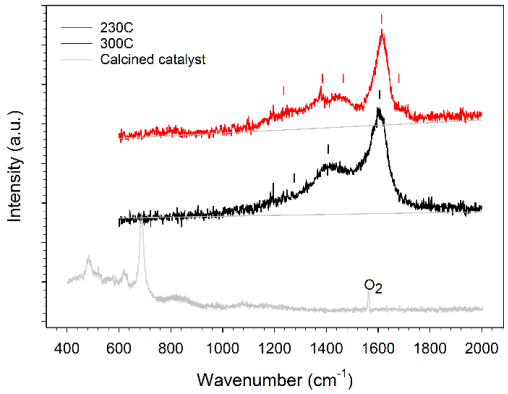

Figure 9. *Raman spectra of the calcined catalyst and carburized catalyst samples at 230 (230C) and 300 °C (300C). 325 nm excitation and 0.3 mW laser power.*

At the applied excitation wavelength (325 nm) an overlap of the basic spectral features of carbon structures is expected [46]. Furthermore, resonance of molecular polycyclic aromatic structures that might act as building blocks of extended carbon structures is also possible at the used wavelength [47]. Here for the carburized samples both of the G and D features are visible. In both cases, the peaks are broad, with significant overlap, possibly due to the existence of several carbon types. Particularly for the 230C sample, a broad band with contributions from at least 3 peaks is visible in the range where the D-peak is expected. As observed by TGA there is a difference in the amount of H_2- resistant carbon structures present in the 230C and 300C samples, the broader D-peak area could be attributed to larger amounts of easily hydrogenated types of carbon that are removed under our reduction conditions at 350 °C.

The characteristics of representative carbon features are presented in **Table 5**, but one should bear in mind that the possible existence of resonance from molecular species might render the obtained values not applicable for the deconvolution of carbon structures. Therefore, the features of the Raman spectra are not sufficient to draw a solid conclusion on the existing carbon types and multi-wavelength approaches have to be applied. Nevertheless, from Raman and TGA analysis we can conclude that the samples contain a diverse range of carbon types.

Table 5. Peak analysis of the Raman spectra.

Sample	D (cm^{-1})	G (cm^{-1})
230C	1462	1617
300C	1416	1608

4. Conclusions

A Re/Co/γ-Al_2O_3 catalyst was exposed to different pre-treatments and the resulting materials were characterized and investigated for their FTS performance. A conventional activation procedure under H_2 was compared with a 3-step activation protocol containing H_2 reduction – CO carburization – H_2 reduction sequence (RCR). The cobalt phases were evaluated by XRD and XANES after each step of the process, while the carbon content and nature of the carbon was studied using TGA-DSC-MS and Raman spectroscopy.

In the first step of the activation procedure Co_3O_4 NPs of the calcined catalyst are reduced under H_2. This step was common in all the examined combinations and resulted in a material with a complex metallic Co^0 structure consisting of both fcc Co and hcp Co and the fcc phase is dominant. Its FTS performance was used as reference for comparing results from the applied RCR activation protocols. After carburization of the reduced catalyst, under pure CO at 14 bar, the Co NPs adapt mainly a Co_2C orthorhombic structure, while significant amount of carbon is co-produced. Carburization at 230 °C produces less H_2 resistant carbon than carburization at 300 °C. After the final H_2 reduction step the Co_2C decomposes to Co NPs with a hcp rich configuration independent of the temperature conditions applied, whereas minor contribution from fcc Co may be observed.

The 3 step RCR activation procedure had a strong impact on the catalyst performance compared to the ordinary H_2 reduction process. Results from FTS experiments show a rather diverse behaviour, including exceptionally desirable as well as very poor performance. In terms of activity and selectivity, the RCR activation has the potential to outperform the classic/conventional reduction when the temperatures of carburization and the final reduction are taking place at low (230 ^oC) and high (350 ^oC) temperatures, respectively. At these conditions a 54% increase in the reaction rate (rCO), a 5% enhancement in C_{5+} selectivity and a remarkable 32% increase in the o/p ratio for the C_3 hydrocarbons are witnessed, when compared to experiments using the conventional H_2 reduction. On the contrary, it becomes clear that at a high carburization temperature (300 ^oC) or a low final reduction temperature (200 ^oC) significantly suppresses the catalytic performance (both in terms of activity and selectivity), although all RCR activated catalysts share a similar hcp-rich catalyst microstructure.

The effect of air exposure of the carburized sample was investigated in detail. It appears that although the bulk crystalline structure of the catalysts doesn't change, minor structural changes occur as observed by *in situ* XANES. A clear performance loss is observed upon exposure to air for the catalyst carburized at low temperature (230 ^oC). The performance of the catalyst carburized at a higher temperature (300 ^oC) and the sample reduced at a low temperature (200 ^oC) are more challenging to interpret. Our results clearly demonstrate that the application of RCR activation protocols combined with O_2 passivation or air exposure with the idea of further use of the material as a precursor in CSTRs or other temperature limited applications probably are not applicable.

Carbon formation is evident after carburization treatments at both temperatures investigated, and H_2 resistant carbon seems to be the cause of the low activity and changes in the selectivity observed here. Results from TGA-DSC-MS and Raman spectroscopy show that several types of carbon structures are present in the samples in addition to the Co_2C that was detected by XRD. The detrimental effect of carbon is not yet fully understood and merits further investigation, especially in relation to selectivity towards higher hydrocarbons since it appears related to the secondary hydrogenation ability of the catalyst, also influencing o/p ratio.

Acknowledgment

The project is funded by Research Council of Norway and Statoil under the GASSMAKS research program (grant no. 215519/E30). NET would like to thank inGAP (Innovative Natural Gas Processes and Products) Centre of Research-based Innovation, which receives financial support from the Research Council of Norway under contract no. 174893. Pablo Beato (Haldor Topsøe A/S) is acknowledged for the valuable discussions. Wouter van Beek (SNBL-BM01B) and the personnel of the Swiss-Norwegian Beamlines are highly acknowledged for experimental assistance (experiment 01-01-965).

References

[1] M.E. Dry, in:, Handb. Heterog. Catal., 2008, pp. 2965–2993.

[2] T.A. Moore, Int. J. Coal Geol. 101 (2012) 36.

[3] E. Iglesia, Appl. Catal. A Gen. 161 (1997) 59.

[4] M.E. Dry, Catal. Today 71 (2002) 227.

[5] E. Rytter, N.E. Tsakoumis, A. Holmen, Catal. Today 261 (2016) 3.

[6] J. Cheng, P. Hu, P. Ellis, S. French, G. Kelly, C.M. Lok, J. Phys. Chem. C 114 (2010) 1085.

[7] E. Rytter, E. Ochoa-Fernández, A. Fahmi, in:, P. Imhof, J.C. van der Waal (Eds.), Catal. Process Dev. Renew. Mater., 2013.

[8] V.A. de la Peña O'Shea, J.M. Campos-Martín, J.L.G. Fierro, Catal. Commun. 5 (2004) 635.

[9] Z. Pan, M. Parvari, D.B. Bukur, Top. Catal. 57 (2014) 470.

[10] O. Ducreux, J. Lynch, B. Rebours, M. Roy, P. Chaumette, in:, Stud. Surf. Sci. Catal., 1998, pp. 125–130.

[11] O. Ducreux, B. Rebours, J. Lynch, M. Roy-Auberger, D. Bazin, Oil Gas Sci. Technol. - Rev. l'IFP 64 (2009) 49.

[12] H. Karaca, O. V. Safonova, S. Chambrey, P. Fongarland, P. Roussel, A. Griboval-Constant, M. Lacroix, A.Y. Khodakov, J. Catal. 277 (2011) 14.

[13] J.C. Mohandas, M.K. Gnanamani, G. Jacobs, W. Ma, Y. Ji, S. Khalid, B.H. Davis, ACS Catal. 1 (2011) 1581.

[14] E. Rebmann, P. Fongarland, V. Lecocq, F. Diehl, Y. Schuurman, Catal. Today 20 (2016) 207.

[15] G. Kwak, M.H. Woo, S.C. Kang, H.-G. Park, Y.-J. Lee, K.-W. Jun, K.-S. Ha, J. Catal. 307 (2013) 27.

[16] L. Braconnier, E. Landrivon, I. Clémençon, C. Legens, F. Diehl, Y. Schuurman, Catal. Today 215 (2013) 18.

[17] M.K. Gnanamani, G. Jacobs, W.D. Shafer, B.H. Davis, Catal. Today 215 (2013) 13.

[18] M. Claeys, M.E. Dry, E. van Steen, E. du Plessis, P.J. van Berge, A.M. Saib, D.J. Moodley, J. Catal. 318 (2014) 193.

[19] D.I. Enache, B. Rebours, M. Roy-auberger, R. Revel, J. Catal. 205 (2002) 346.

[20] L.J.E. Hofer, W.C. Peebles, J. Am. Chem. Soc. 69 (1947) 2497.

[21] S. Weller, L.J.E. Hofer, R.B. Anderson, J. Am. Chem. Soc. 70 (1948) 799.

[22] L.J.E. Hofer, E.M. Cohn, W.C. Peebles, J. Phys. Colloid Chem. 53 (1949) 661.

[23] Hendrik Van Rensburg, U.S. Patent, 9387463 B2, 2016.

[24] P.H. Emmett, J.F. Shultz, J. Am. Chem. Soc. 51 (1929) 3249.

[25] J.-X. Liu, H.-Y. Su, D.-P. Sun, B.-Y. Zhang, W.-X. Li, J. Am. Chem. Soc. 135 (2013) 16284.

[26] R.C. Reuel, C.H. Bartholomew, J. Catal. (1984) 63.

[27] F. Diehl, A.Y. Khodakov, Oil Gas Sci. Technol. - Rev. l'IFP 64 (2008) 11.

[28] N.E. Tsakoumis, A. Voronov, M. Rønning, W. Van Beek, Ø. Borg, E. Rytter, A. Holmen, J. Catal. 291 (2012) 138.

[29] B. Ravel, M. Newville, J. Synchrotron Radiat. 12 (2005) 537.

[30] Y. Joly, Phys. Rev. B 63 (2001) 125120.

[31] A.P. Hammersley, S.O. Svensson, M. Hanfland, A.N. Fitch, D. Hausermann, High Press. Res. 14 (1996) 235.

[32] P. Scherrer, Gottingen Nachrichten 2 (1918) 98.

[33] G.S. Pawley, J. Appl. Crystallogr. 14 (1981) 357.

[34] M. Wojdyr, J. Appl. Crystallogr. 43 (2010) 1126.

[35] A. Coelho, (2008) Topas V4.2 (Bruker AXS).

[36] E. Patanou, A.H. Lillebø, J. Yang, D. Chen, A. Holmen, E.A. Blekkan, Ind. Eng. Chem. Res. 53 (2014) 1787.

[37] E.A. Blekkan, Ø. Borg, V. Frøseth, A. Holmen, Catal. - R. Soc. Chem. 20 (2007) 13.

[38] M. Rønning, N.E. Tsakoumis, A. Voronov, R.E. Johnsen, P. Norby, W. van Beek, Ø. Borg, E. Rytter, A. Holmen, Catal. Today 155 (2010) 289.

[39] G.L. Bezemer, J.H. Bitter, H.P.C.E. Kuipers, H. Oosterbeek, J.E. Holewijn, X. Xu, F. Kapteijn, A.J. van Dillen, K.P. de Jong, J. Am. Chem. Soc. 128 (2006) 3956.

[40] E. Rytter, N.E. Tsakoumis, A. Holmen, Catal. Today 261 (2016) 3.

[41] D. Lee, J. Lee, S. Ihm, Carbon N. Y. 36 (1988) 199.

[42] D. Moodley, J. van de Loosdrecht, H. Niemantsverdriet, A.M. Saib, in:, 2009.

[43] C.H. Bartholomew, Catal. Rev. 24 (1982) 67.

[44] H. Knözinger, G. Mestl, Top. Catal. 8 (1999) 45.

[45] Y. Inada, T. Amaya, T. Hirao, RSC Adv. 5 (2015) 18523.

[46] A.C. Ferrari, J. Robertson, Phys. Rev. B 64 (2001) 75414.

[47] C.R. Johnson, S.A. Asher, Anal. Chem. 56 (1984) 2258.